Analyst

Overcoming Aggregation with Laser Heated Nanoelectrospray Mass Spectrometry: Thermal Stability and Pathways for Loss of Bicarbonate from Carbonic Anhydrase II

1
2
3
4
5
6
7
8
9
10
11
12
13
14
15
16
17
18
19
20
21
22
23
24
25
26
27
28
29
30
31
32
33
34
35
36
37
38
39
40
41
42
43
44
45
46
47
48
49
50
51
52
53
54
55
56
57
58
59
60

Overcoming Aggregation with Laser Heated Nanoelectrospray Mass Spectrometry:

Thermal Stability and Pathways for Loss of Bicarbonate from Carbonic Anhydrase II

Jacob S. Jordan, Katherine J. Lee, and Evan R. Williams

Department of Chemistry, University of California, Berkeley, California, 94720-1460

*To whom correspondence should be addressed

e-mail: erw@berkeley.edu

Abstract

Variable temperature electrospray mass spectrometry is useful for multiplexed measurements of the thermal stabilities of biomolecules, but the ionization process can be disrupted by aggregation-prone proteins/complexes that have irreversible unfolding transitions. Resistively heating solutions containing a mixture of bovine carbonic anhydrase II (BCAII), a CO_2 fixing enzyme involved in many biochemical pathways, and cytochrome c leads to complete loss of carbonic anhydrase signal and a significant reduction in cytochrome c signal above ~72 °C due to aggregation. In contrast, when the tips of borosilicate glass nanoelectrospray emitters are heated with a laser, complete thermal denaturation curves for both proteins are obtained in <1 minute. The simultaneous measurements of the melting temperature of BCAII and BCAII bound to bicarbonate reveal that the bicarbonate stabilizes the folded form of this protein by ~6.4 °C. Moreover, the temperature dependences of different bicarbonate loss pathways are obtained. Although protein analytes are directly heated by the laser for only 140 ms, heat conduction further up the emitter leads to a total analyte heating time of ~41 s. Pulsed laser heating experiments could reduce this time to ~0.5 s for protein aggregation that occurs on a faster time scale. Laser heating provides a powerful method for studying the detailed mechanisms of cofactor/ligand loss with increasing temperature and promises a new tool for studying the effect of ligands, drugs, growth conditions, buffer additives, or other treatments on the stabilities of aggregation-prone biomolecules.

Introduction

Proteins typically function in one or more "native" conformations[1] that can be affected by solution properties including the pH,[2,3] ionic strength,[4–6] co-solutes such as ions,[6–8] other proteins or macromolecular crowding agents,[4,9,10] pressure,[11–13] and temperature.[14,15] Protein misfolding can result in aggregation-prone conformations, which are associated with a wide range of human diseases.[16] Thermal stability measurements or melting temperatures (T_m) are often used to determine how stable native protein complexes/conformations are relative to unfolded or misfolded states, which helps to predict how ligands may bind to certain structures, how enzymes may function under certain conditions, and how long protein therapeutics are stable when stored in different buffers. A number of biophysical assays are routinely used to study the thermal stabilities of proteins, protein complexes, and protein-ligand interactions, including circular dichroism,[14,17] differential scanning calorimetry,[17–19] differential scanning fluorimetry,[20,21] or ultraviolet/visible (UV/Vis)-spectrophotometry.[15,17] Fluorescence-based and calorimetric assays are routinely used to study the aggregation temperature of monoclonal antibodies and other biotherapeutic complexes from different buffer conditions.[21–24] However, all of these methods generally require purified samples and do not provide the type of detailed information that mass spectrometry (MS) can provide about solution conformers, unfolding intermediates, or ligand-binding.

Native MS is a well-established technique for measuring the stabilities of proteins and protein-ligand binding interactions.[25–29] It is possible to unambiguously identify ligand-binding from samples containing a single protein and thousands of potential ligands.[30] MS-based methods of measuring protein thermal stabilities have the advantage that they are sensitive and can be used to investigate protein mixtures as long as proteins have different masses that can be

resolved.[31–33] Protein melting curves are obtained from MS data by monitoring the average

charge state of each analyte or the relative abundance of conformers identified by ion mobility

spectrometry. Variable-temperature electrospray ionization (vT-ESI), in which the solution

temperature is varied during electrospray, has been used to determine the T_m values of

proteins,[34–39] protein complexes,[19,34,40–46] protein as well as DNA complex unfolding

pathways,[42,47–49] and the thermochemistry of ligand-binding to protein- and DNA-ligand

complexes.[38,47,50,51] In combination with ion mobility spectrometry, thermochemical values can

be determined for individual groups of closely related protein conformers.[36,38,40,52,53] The T_m

values of 7 analyte molecules from a mixture of proteins was determined simultaneously,[54]

clearly demonstrating the multiplexing capacity of this technique. Measurements with vT-ESI

can be time consuming owing to the time necessary for thermal equilibration at each

temperature. However, recent results demonstrate the acquisition of full melting curves for

model proteins in <1 min.[39] Rapid heating of a solution on timescales between 0.8 ms – 4

minutes can also be done using theta glass emitters[55] or by rapidly flowing a solution through a

resistively heated portion of an emitter.[35,47]

Protein melting has also been investigated using laser heating, either by irradiating the end of

electrospray emitters[56–58] or by heating electrospray droplets directly.[38,59] Heating the end of a

100 μm diameter metal emitter led to protein unfolding and dissociation of noncovalent

biomolecular complexes.[56,57,60] Heating the end of borosilicate emitters has the advantage that

the solution temperature can be rapidly changed due to the small solution volume and rapid heat

transfer to the surrounding atmosphere.[58] Solutions can be heated from room temperature to ~78

°C in less than 0.5 s and cooled from ~82 °C back to room temperature in <4 s.[58] The rapid

equilibration enables acquisition of protein melting curves in <40 s and laser power can be

converted to solution temperature by calibration with vT-ESI data.[58] By laser heating

electrospray droplets, unfolding intermediates were kinetically trapped and analyzed by ion

mobility spectrometry.[38,59] Multiple time points along the unfolding process were measured

using electrospray emitters with different diameters to produce droplets with different lifetimes.

These laser-based heating techniques show great promise for rapidly characterizing protein T_m

values, but to date, full melting curves have only been acquired for model proteins that have

reversible unfolding transitions.

It is challenging to identify the T_m values of proteins that aggregate quickly with vT-ESI

because of ion signal loss.[40,42] Here, the *rapid, localized* heating of laser-heated electrospray

ionization (LH-ESI) enables, for the first time, detailed information about the thermal

denaturation and bicarbonate loss mechanisms of bovine carbonic anhydrase II, a protein that

rapidly aggregates at high temperatures, to be obtained. The effect of the bound bicarbonate

reaction product on the thermal stability of the protein can also be obtained simultaneously from

the same solution. The ability to measure melting transitions before aggregation can disrupt the

electrospray process expands the multiplexing capacity of MS-based measurements of protein

thermal stabilities to include mixtures containing aggregation-prone components, a class which

includes monoclonal antibodies and other important biotherapeutics.

Materials and Methods

An LH-ESI source with a Synrad F48-2 10.6 μm CO_2 laser (Synrad Corporation,

Mukilteo, WA) was used to heat the end of borosilicate glass electrospray emitters.[58] The length

of the tip that was heated was limited with a metal beam block. Electrospray emitters were

positioned in the beam using a 3-axis stage and a Dino-Lite digital microscope (Torrance, CA)

such that either the final 300 μm or 500 μm of the tip was positioned past the beam block. An IR

power meter head (Ophir-Spiricon, Logan, UT) was positioned downstream of the laser beam

after the capillary to measure the laser power in real time. An Arduino Due microcontroller

(Somerville, MA) was used to control and record the laser power during the experiment via

Arduino and Python code. An electrospray voltage of +1.3 – 1.7 kV was applied to a platinum

wire that was inserted into the back of the capillary and was in contact with the solution.

A vT-ESI source similar to that of Sterling et al.[61] was constructed for comparison to LH-

ESI data. In brief, the source consists of an aluminum cylinder wrapped with resistive heating

wire. The temperature of the apparatus is measured using a J-type thermocouple and an Omega

CNi-3222 temperature controller (Stamford, CT). A thermocouple placed in the tip was used to

calibrate the temperature measured inside of the heating jacket to a solution temperature.

Electrospray emitters were inserted through the front end of the source until the emitter tip was

aligned with the end of the heating jacket. The temperature of the apparatus was equilibrated for

~70 s at each temperature prior to starting electrospray at 1.3 kV. Data were acquired for ~10 s at

each temperature for analysis. The custom LH-ESI or vT-ESI sources were aligned at the inlet of

an Orbitrap Elite mass spectrometer (Thermo Fisher Corporation, Waltham, MA). Mass spectra

were acquired between $m/z = 500 – 4000$ at a resolution setting of 15,000 to improve

transmission of high m/z ions.

Nanoelectrospray emitters were pulled from borosilicate glass capillaries (1.0 mm outer

diameter, 0.78 mm inner diameter, Sutter Instrument, Novato, CA, Part no. BF100-78-10) to a

final inner diameter of 2.45 ± 0.30 μm using a P-87 Flaming/Brown micropipette puller (Sutter

Instrument).[62] Emitters were imaged using a Hitachi TM-1000 (Tokyo, Japan) scanning electron

microscope at the Electron Microscopy Laboratory at the University of California, Berkeley.

Emitter flow rates were determined by measuring the mass of the emitter loaded with ~5-10 μL of solution using an Ohaus Analytical Plus balance (Parsippany, NJ) before and after electrospray at 1.3 kV for 5 minutes.[63,64] To determine the mass loss due to evaporation, the same emitter was placed in front of the mass spectrometer with no spray voltage applied and the mass was measured after 5 minutes. Mass loss due to solution flow during electrospray and evaporation were obtained using a density of 0.99821 g/mL for water at 20 °C.[65]

Bovine carbonic anhydrase II (BCAII) and cytochrome *c* (cyt *c*) solutions were prepared 7:3 in 50 mM ammonium acetate to a total protein concentration of 10 μM in Milli-Q water. All reagents were obtained from Sigma-Aldrich (St. Louis, MO) and were used without further purification. All reported melting curves, melting temperatures, and flow rates are the average of three replicate measurements using different ESI emitters.

Results and Discussion

Comparison of vT-ESI and LH-ESI for BCAII and Cyt c Melting Measurements.

Bovine carbonic anhydrase II (BCAII) is a well-studied protein responsible for catalyzing the reversible hydration of CO_2 to ionic bicarbonate, a critical function in living organisms.[66] This protein is also a model system for understanding biochemical CO_2 reduction, knowledge that could lead to viable methods for converting CO_2 to useful chemical precursors.[67] However, industrial applications for BCAII are limited by the thermal stability of the enzyme,[67] which undergoes extensive aggregation in <5 min at 63 °C.[9] To gain insight into the stability of this important enzyme at elevated temperatures, vT-ESI was used to study the melting process of BCAII and the model protein cyt *c* that reversibly melts. A typical native mass spectrum acquired from a 50 mM aqueous ammonium acetate solution containing 7 μM BCAII and 3 μM

7

cyt c is shown in Figure 1a. Both protonated (29,087.9 ± 0.8 Da)[68] and bicarbonate-bound (+61.1 ± 2.1 Da) BCAII with the native Zn^{2+} cofactor are formed (Figure 1a, inset). Ionic bicarbonate is a reaction product of BCAII catalytic activity and has previously been observed to be bound to BCAII in native MS experiments.[68] The tailing to higher m/z from the bicarbonate-bound form of BCAII is due to small nonspecific adducts that remain under the low inlet temperatures used in these experiments (100 °C) to prevent inadvertent heating of solution in the ESI emitters. The +6 - +8 charge states of cyt c are also formed, consistent with prior results.[35,58,69]

The melting of BCAII and cyt c was measured between solution temperatures of 27 °C and 86 °C using vT-ESI. At ~64 °C, there is a small population of higher charge states corresponding to unfolded BCAII (Figure 1b). No BCAII signal is observed at temperatures greater than ~72 °C (Figure 1d, data at 68 °C shown). There is an increase in light scattering intensity at 500 nm in <300 s when solutions of ~7 μM BCAII in 50 mM potassium phosphate buffer (pH 7) are incubated at 63 °C,[9] indicating that BCAII aggregates to form large oligomers at high temperatures. This indicates that the decrease in BCAII signal in these vT-ESI measurements above ~64 °C is due to aggregation. Cyt c ions are still observed at temperatures >75 °C (Figure 1d, data at 68 °C shown), but remarkably, there are no high charge states of cyt c at 75 °C or even higher temperatures that are well above the melting temperature of this protein (T_m = ~74 °C).[35,70] Moreover, the abundances of the low charge states of cyt c are considerably lower at temperatures above 65 °C compared to when BCAII is not present in solution. The absence of unfolded monomers of cyt c indicate that these species may be co-aggregating with unfolded monomers of BCAII. Cyt c signal becomes highly variable above ~68 °C (Figure S1a). This suggests that aggregation may affect the ESI ion formation process at these relatively small emitter tip sizes. The complete loss of signal for BCAII, but not for cyt c, indicates that the

aggregation process is rapid and produces large oligomers that are outside the mass or detection limits of the mass spectrometer.

LH-ESI is advantageous over vT-ESI due to rapid thermal equilibration times and localized heating at the very end of the emitter leading to less time for unfolded proteins to aggregate in solution. To investigate whether melting curves could be obtained before aggregation interferes with the electrospray process, the same BCAII/cyt c mixture was rapidly heated in the tip of the electrospray emitter using an LH-ESI source. Just the final 300 μm of the emitter tip was heated by using a beam block to limit the length of the capillary that was irradiated by the laser. The laser power was ramped between 0 W (laser off) and ~3.9 W. The laser powers used here are higher than those used in prior LH-ESI experiments due to irradiating a shorter, thinner volume at the end of the emitter tip.[58]

The mass spectra did not change with laser powers below ~1.8 W. At ~1.8 W, higher charge state ions (+11 - + 31) corresponding to denatured BCAII appear. These high charge state ions increase in abundance with increasing laser power (Figure 1c,e) and above ~3.3 W the abundances of all BCAII ions decrease (Figure 1e, S1b). The abundance of cyt c also increases with increasing laser power, reaching a maximum at the highest laser power of ~3.9 W used here (Figure S1b). Increased protein signal with increasing laser power was reported in "laser spray" experiments and was attributed to enhanced desolvation at the tip of the emitter at high solution temperatures.[56] The tailing baseline to higher m/z for the native charge states of BCAII at room temperature is largely eliminated at higher temperatures. This indicates that the adducts that cause the tailing are weakly bound to the protein. Solutions were prepared from lyophilized samples. During lyophilization, the concentration of material in solution, including salts and small molecules, increases and can lead to binding or adduction with the protein prior to or at the

time the lyophilized powder is formed. Upon rehydration, these species may stay bound for a

long period of time even in dilute solution. This adduction is not observed after turning the laser

off and allowing the solution to cool back to room temperature (Figure S2a,b). At high solution

temperatures, these weakly bound adducts may be lost from the protein and diffuse into the

relatively dilute solution, preventing their rapid reassociation with the protein after the solution

returns to room temperature. These results indicate that laser heating may be used to reduce

adduction for more accurate and sensitive mass measurements.

At laser powers >3.7 W, there are no BCAII ions. We attribute the decrease in ion signal at

higher laser power to rapid aggregation. Turning the laser off results in a return to a native

charge state distribution and the re-appearance of peaks corresponding to BCAII in ~42 s

resulting in spectra that are the same as that shown in Figure 1a (without adduction to BCAII

ions, Figure S2b,c). These data indicate that fast heating with LH-ESI enables the analysis of the

melting behavior of aggregation-prone proteins before aggregation can clog the spray or deplete

the abundance of the monomer, expanding MS-based thermal stability measurements to a much

wider range of biomolecular analytes.

Melting Curves for vT-ESI and LH-ESI Data

Melting curves are constructed from temperature dependent data by monitoring the change in

the average charge state (ACS) or changes in the relative abundance of individual charge

states/ion mobility identified conformers. For vT-ESI, the ACS of BCAII increases from $9.58 \pm$

0.08 to a maximum of 13.94 ± 0.54 between ~27 °C and ~72 °C (Figure 2a, blue data) after

which no protein signal was obtained. The ACS of cyt *c* increases slightly from 6.96 ± 0.01 at

~27 °C to 7.38 ± 0.09 at ~86 °C (Figure 2a, orange data). The maximum ACS of cyt *c* in a

mixture with BCAII at 86 °C is significantly lower than the maximum ACS obtained from

solutions containing only cyt *c* (11.05 ± 0.30 at ~90 °C, Figure 2a, black data).[3] Essentially no

information about the melting behavior of cyt *c* or BCAII can be obtained from these vT-ESI

experiments due to the co-aggregation initiated by BCAII at ~64 °C.

Protein melting data acquired by LH-ESI can also be used to construct melting curves as a

function of laser power. The ACS of BCAII increases from 9.76 ± 0.11 at 0 W to 17.62 ± 0.55 at

~3.6 W (Figure 2b, blue data). The ACS of cyt *c* increases from 6.97 ± 0.03 at 0 W to 8.69 ±

0.23 at ~3.9 W (Figure 2b, orange data). The maximum ACS of BCAII at ~3.6 W of laser power

(17.62 ± 0.55) is significantly higher than the ACS at ~64 °C (13.94 ± 0.54) with vT-ESI,

indicating that melting is not completed in vT-ESI before BCAII oligomerization interferes with

the thermal stability measurements. The average charge state of cyt *c* at ~3.9 W is lower than the

previously reported maximum average charge state for cyt *c* from vT-ESI experiments.[58] This is

consistent with some population of denatured cyt *c* monomers co-aggregating with BCAII at

very high laser powers, as was the case with vT-ESI, reducing the high charge population and

reducing the ACS.

The average charge state versus laser power data were fit to a two-state model and resulted

in melting power (P_m) values of ~2.6 W and ~3.3 W for BCAII and cyt *c,* respectively (Figure

2b). At high laser powers, the loss of BCAII ion signal indicates that the rate of aggregation is

substantially higher and that aggregation occurs more rapidly than the residence time scale of

solution in the heated portion of the emitter tip prior to electrospray droplet formation.

The unfolding transition of cyt *c* can be used to calibrate the laser power to solution

temperature in LH-ESI experiments.[58] This method works best over the temperature range where

the change in the average charge state versus temperature is highest. In the case of cyt *c*, this

region (~3.0 - 3.6 W) does not have appreciable overlap with the melting transition of BCAII

(~1.7 – 3.0 W). Therefore, a new calibration method was devised that uses the cyt *c* melting

transition to determine the maximum temperature in the emitter tip before BCAII aggregation

(Figure S3a,b). Then, the BCAII melting curve determined by LH-ESI was mapped between

room temperature and this maximum value to generate a linear calibration function for

converting laser power to solution temperature (Figure S3c,d). This two-protein calibration

results in T_m values of 63.4 ± 0.6 °C and 73.9 ± 0.5 °C for BCAII and cyt *c* (Figure 2b, top axis),

respectively, in agreement with the reported melting temperatures for these proteins (~63 °C[9,71]

and ~74 °C,[35,54,58,70] respectively) obtained by circular dichroism and UV/Vis-

spectrophotometry. Thermal stabilities of multiple proteins that have reversible unfolding

transitions can be measured simultaneously using vT-ESI and LH-ESI.[54,58] Our data indicate that

if one of the proteins in solution aggregates upon unfolding, it may not be possible to obtain

melting temperatures even for proteins that have reversible unfolding transitions and that adverse

effects of aggregation and co-aggregation in protein mixtures can be overcome using LH-ESI.

Effect of the Bicarbonate Ion on BCAII Thermal Stability

  MS-based measurements of protein melting have the advantage that the thermal

stabilities of multiple forms of a protein with different masses, such as post-translational

modifications and ligand- or cofactor-bound species, can be obtained simultaneously.[31] LH-ESI-

MS results enable the concurrent analysis of the thermal stability of Zn-bound BCAII with and

without a bound bicarbonate reaction product because the masses of these ions differ by ~61 Da

(Figure 1a, inset).[68] With vT-ESI, there is a slight increase in the ACS of bicarbonate-bound

BCAII species from 9.46 ± 0.08 at 27 °C to a maximum of 10.74 ± 0.84 at 64 °C (Figure 2a, red

data), but the full melting behavior of this species cannot be tracked because there are no

detectable BCAII ions above ~72 °C. The melting behavior of the apo- and bicarbonate-bound

forms of the protein can be determined by LH-ESI. The ACS of bicarbonate-bound BCAII

increases from 9.59 ± 0.22 at ~27 °C (0 W) to 16.92 ± 0.82 at ~79 °C (~3.6 W) (Figure 2b, red

data). These data can be fit to a two-state model with a T_m of 69.8 ± 1.0 °C ($P_m = 3.01 \pm 0.07$

W), which is higher than the T_m of the apo-protein (63.4 ± 0.6 °C, $P_m = 2.55 \pm 0.04$ W). The 6.4

°C higher T_m value for bicarbonate-bound BCAII compared to the apo-protein indicates that the

bicarbonate ion significantly stabilizes the folded conformation of BCAII.

Thermal denaturation of BCAII has been measured using a variety of biophysical

characterization methods, including UV/Vis-spectrophotometry, differential scanning

calorimetry, differential scanning fluorimetry, and circular dichroism. A T_m value of ~62 - 64

°C[66,71,72] obtained by these methods corresponds well with the measured T_m of apo-BCAII in the

LH-ESI experiments. The thermal stability of an enzyme can also be measured by monitoring the

enzymatic activity as a function of temperature. BCAII catalyzes the formation of a bicarbonate

ion from CO_2 and the enzymatic activity can be assessed by monitoring the pH change in a

slightly alkaline (pH ~8.1) CO_2-saturated solution to more neutral conditions (pH ~7) using a

pH-sensitive dye or pH meter.[66,73,74] BCAII also exhibits esterase activity, which can be readily

assessed by an increase in absorbance by the formation of *p*-nitrophenolate from the ester

substrate *p*-nitrophenyl acetate.[66,75] Across a range of buffer conditions, a sharp decrease in both

CO_2 hydration and esterase activity occurs at ~60 - 65 °C.[73–75] This is consistent with the thermal

denaturation temperature of apo-BCAII and indicates that thermal denaturation is concomitant

with loss of enzymatic activity. The residual activity of this enzyme at 70 °C has been reported to

be between 0 – 30% at 25 °C,[72–75] consistent with some residual folded BCAII at this

temperature. Conventional biophysical techniques used to measure protein thermal stability

cannot distinguish between the apo- and holo-forms of the protein. Because LH-ESI-MS can

independently monitor the unfolding of the apo- and bicarbonate-bound forms of BCAII by a

difference in mass, this method is uniquely suited for studying the complex thermal denaturation

and bicarbonate loss mechanisms of this enzyme.

Energetics and Mechanism for Loss of Bicarbonate from BCAII

Changes in the ACS vs temperature provide information about the difference between the

thermal stabilities and T_m values of the bicarbonate-bound and apo-forms of BCAII, but do not

provide mechanistic information about bicarbonate loss, the rate of interconversion between the

two forms during heating, or the thermal stability of the protein-bicarbonate interaction. To

investigate these properties of BCAII melting, the relative abundance of the folded (+8 - +10

charge states) and denatured (+11 - +31 charge states) forms of bicarbonate-bound and apo-

BCAII were compared as a function of laser power. Unfolding of small proteins, such as BCAII,

is typically fast on the time scale of these experiments. Under these conditions, mechanistic

information about the ligand loss process can be derived from temperature-dependent

measurements.

Changes in the ACS of the folded (F) and unfolded (U) forms of apo-BCAII measured by

LH-ESI-MS show a melting temperature for the transition F → U of 63.4 ± 0.6 °C. Similarly, the

ACS indicates a melting temperature for the transition of folded (BF) to unfolded (BU)

bicarbonate-bound BCAII of 69.8 ± 1.0 °C. However, there are three pathways that can

potentially occur for BF → U (Scheme 1). Information about these pathways can be obtained

from analysis of the temperature dependance of the relative abundances of all the different forms

of this protein. These data obtained with LH-ESI-MS are shown in Figure 3. Initially, folded

apo- (F) and bicarbonate-bound BCAII species (BF) are predominant but their abundances

decrease from $35.8 \pm 1.7\%$ and $58.1 \pm 1.5\%$ at room temperature (0 W) to ~1% at ~78 °C (~3.6

W), respectively (Figure 3, blue and red data, respectively). A two-state model fit to the data

results in T_m (P_m) values of 65.1 ± 1.0 °C (2.68 ± 0.07 W) and 63.4 ± 0.5 °C (2.56 ± 0.04 W),

respectively. The T_m for depletion of BF (63.4 ± 0.5 °C) is lower than the T_m determined for BF

→ BU from changes in the ACS (69.8 ± 1.0 °C). This is because the former includes both

pathways for depletion of BF via BF → U and BF → BU → U whereas the latter is specific for

BF → BU. The adequate fit of the F → U process to a sigmoidal curve and the absence of a

measurable increase in F with temperature indicates that the process BF → F does not occur with

F as a stable intermediate to any considerable extent. While this process may occur at

temperatures above 63 °C, the lack of an increase in F indicates that F that is formed by

bicarbonate loss at this elevated temperature is not stable on the time scale of our experiments.

The relative abundance of BU increases with temperature, reaches a maximum, and

subsequently decreases at higher temperature indicating BU must go to U (Figure 3, green data).

This is confirmed by the high abundance of U with increasing temperature which indicates that a

substantial fraction of U must come from BF as well as F. The relative abundance of U increases

from $2.8 \pm 1.5\%$ at ~27 °C to $85.9 \pm 5.3\%$ at ~80 °C with a formation temperature (T_f) of $65.8 \pm$

0.6 °C (Figure 3a, orange data). The BU data was fit to a sigmoid with sloped baselines to

account for bicarbonate loss at high temperatures and a T_f of 63.8 ± 6.9 °C was obtained (Figure

3a, green data). This value is similar to the value obtained for F → U using the ACS method.

In order to separate the different pathways for formation of U from the LH-ESI melting

curve data, the theoretical pathway BF → BU was modeled by assuming 100% conversion of BF

to BU with no direct formation of U (Figure 3b, red dashed line). The difference between the theoretical and observed abundance of BU must be due to loss of bicarbonate from the unfolded bicarbonate-bound protein at high temperatures (BU → U) (Figure 3b, green dashed line). Fitting these data to a two-state model gives a T_m value for the BU → U process of ~65.9 °C (Scheme 1).

Formation of U can also proceed directly from BF (BF → U). U must also be formed from F (Figure 3b, blue dashed line, Figure S4) which may account for up to ~36% of U at the highest temperature. The fraction of U that is formed by BF → U can be determined from the difference between the observed abundance of U and the sum of the other two formation pathways for U, F → U and BU → U (Figure S4). The difference between these two functions can be fit to a two-state model with a T_f of ~70.4 °C (Figure S4, black dashed line), indicating that BF → U is a minor, but clearly distinguishable pathway with ~6% relative abundance at ~80 °C. These data indicate that both BF → U and BF → BU are viable pathways for protein unfolding at solution temperatures near the T_m of the bicarbonate-bound protein.

Measuring the melting behavior of proteins using either the ACS or relative abundance of different species can probe different processes that occur during thermal denaturation and loss of a ligand from a protein. The T_m values determined for the F → U process are similar between the two analysis methods (63.4 ± 0.6 °C and 65.1 ± 1.0 °C for ACS and relative abundance quantification, respectively). This is expected because F → U is the only pathway for reducing the abundance of F. In contrast, BF has three potential pathways for loss of abundance. Analysis of temperature-dependent changes in the ACS of the bicarbonate-bound protein monitors *only* the thermal denaturation transition of BF → BU and, as a result, can provide a T_m value for this process. In contrast, the T_m value for the BF → BU process cannot be determined from changes

in the relative abundance of BF due to additional dissociation and unfolding pathways that affect

the observed abundances of BF, BU, and U (BF → BU → U and BF → U). The BU → U

pathway (T_m = ~65.9 °C) influences the BF → BU equilibrium by reducing the abundance of BU

at temperatures greater than ~65 °C. This process shifts more BF to BU, resulting in a lower T_m

for BF determined from relative abundance data (T_m = 63.4 ± 0.5 °C) than from changes in the

ACS (T_m = 69.8 ± 1.0 °C). This method for distinguishing pathways for loss of a ligand should

work when the onset temperatures for the two processes are close, such as the ~4 °C difference

measured here for the BU → U and BF → U pathways (T_m = ~65.9 °C and ~70.4 °C,

respectively).

These LH-ESI-MS data reveal a complex melting behavior that would be challenging to

measure with conventional biophysical characterization techniques that rely on a single

spectroscopic or thermodynamic readout for an ensemble of molecules in a sample. The

description of bicarbonate loss mechanisms outlined above can be elucidated by LH-ESI-MS due

to the ability to distinguish between bicarbonate-bound and apo-forms of BCAII by mass and to

measure melting behavior before substantial aggregation can occur. These data highlight the

importance of analyzing both the ACS and relative abundance of protein species in MS-based

analyses of protein thermal stabilities, which is uniquely suited for the detailed characterization

of temperature-induced ligand loss and protein denaturation mechanisms.

Thermal Timescales of LH-ESI and vT-ESI

An important difference between vT-ESI and LH-ESI is that LH-ESI employs *fast, localized*

heating at the tip of the emitter. Proteins are only heated for a short time prior to formation of

electrospray droplets, which minimizes any aggregation that may occur upon protein unfolding.

17

Once in the electrospray droplet, conditions where there is only one or zero molecules can be readily achieved with small emitter tips or lower protein concentration so that aggregation can be prevented entirely in the droplets.[76–79] In contrast, long thermal equilibration times typically used for vT-ESI can provide enough time for a protein to oligomerize. As noted by a reviewer, a rapid temperature rise could potentially be accompanied by an increase in pressure that can also affect protein structure. However, the emitters are operated at and open to atmospheric pressure at both ends and the laser used in this study has a rise time of well over 1 μs. Thus, the solution pressure should not change during these laser heating experiments and the observed changes in protein structure should be due only to thermal effects.

In order to obtain an estimate of the time that a protein spends in the solution that is directly heated by the laser, the solution flow rate and volume in the heated portion of the emitter were measured. The flow rate was measured gravimetrically,[63,64] and the volume of the tip was approximated by a truncated cone. The inner diameter of the emitter tip and the inner diameter 300 μm away from the tip are ~2.4 μm and ~45 μm determined from scanning electron and optical light microscope images, respectively. The volume of solution in the final 300 μm of the emitter tip is ~170 pL. Solvent evaporation from 2.4 μm emitters occurs at a rate of 15.6 ± 5.9 nL min^{-1}. The flow rate during electrospray after accounting for solvent loss due to evaporation was 73.0 ± 19.0 nL min^{-1}. Based on these values, protein analytes are exposed to the solution that is directly heated by the laser for only ~140 ms prior to electrospray droplet formation. Increasing the heated length of the capillary to 500 μm leads to an increase in the solution volume that is directly heated to ~445 pL, resulting in a protein residence time of ~367 ms.

In addition to the small solution volume that is directly heated by the laser, heat transfer to solution that is not directly heated occurs. Heating the final 300 μm of the emitter to ~82 °C

(~3.9 W) with the laser leads to loss of signal for BCAII. When the laser is turned off, native

BCAII monomer signal returns within 41 ± 26 s (Figure S2c). Thus, a total solution volume of

~50 nL is heated. These results indicate that aggregation of BCAII occurs faster than ~41 s above

~80 °C, which is faster than has been previously reported for this protein. There are likely two

contributing factors. A prior light scattering method could only detect aggregates larger than

~500 nm,[9] whereas depletion/formation of the different conformers of the protein monomer are

measured with MS. Even small aggregates are well outside of the mass range and detection

limits of the Orbitrap mass spectrometer used in this study. Another contributing factor may be

that the rate of protein aggregation increases rapidly with increasing temperature,[80,81] and the

laser heating experiments can take the protein well above its melting temperature.

Heating a longer length of the emitter (500 μm) results in all protein signal disappearing in

<2 s at laser powers of ~0.6 W, indicating that proteins have sufficient time to undergo

aggregation within the emitter before being ejected into electrospray droplets. When this larger

solution volume is heated until protein signal disappears, native charge states return to the same

intensities as before heating after ~74 ± 21 s, corresponding to a total heated volume of ~90 nL.

Indirect heating affects a ~2x larger volume of solution when the final 500 μm of the tip is

heated vs the final 300 μm. This in turns provides a correspondingly longer timescale for protein

aggregation to occur before electrospray droplet formation. Pulsed laser heating can raise the

solution temperature in less than 0.5 s,[58] and could extend these kinetic measurements to proteins

that aggregate in under one second.

Conclusions

A laser can rapidly heat small volumes of solution at the end of a borosilicate ESI

emitter, making it possible to measure the thermal denaturation of aggregation-prone proteins

from which information about the thermal stabilities of protein-ligand interactions and ligand

loss can be obtained. These data show that at moderate solution temperatures where unfolding

and ligand loss begins to occur, the rate at which aggregation occurs is slower than the time

necessary for heating and droplet formation. This enables investigation into the melting behavior

of BCAII in its bicarbonate-bound and apo-forms and the stability of both forms are obtained

simultaneously from the same solution. Analysis of these data using both the average charge

states of individual species as well as the relative abundances of all species makes it possible to

obtain thermochemical information about various pathways for unfolding and ligand loss. The

ability of the LH-ESI method to measure the thermal stability of biomolecules should be

applicable to a wide range of proteins that are prone to aggregation, which includes important

biopharmaceuticals, such as monoclonal antibodies and antibody-drug conjugates. LH-ESI may

also be used to study aggregation kinetics at fast timescales by varying the length of the emitter

heated by the laser beam, providing information about the earliest stages of protein aggregation

and identifying stable intermediate structures amenable to disruption or therapeutic intervention

along the pathway towards higher order oligomers.

LH-ESI also shows significant promise for coupling with solution-phase separations

methods, such as capillary electrophoresis or size exclusion chromatography, where

chromatographic peak widths are <1 minute and shorter than typical thermal equilibration times

necessary to obtain vT-ESI data over a full range of temperatures. Obtaining LH-ESI melting

curves on chromatographic timescales would add an additional dimension of information to

native MS analyses of complex mixtures. In combination with autosampling instrumentation,

1
2
3
4
5
6
7
8
9
10
11
12
13
14
15
16
17
18
19
20
21
22
23
24
25
26
27
28
29
30
31
32
33
34
35
36
37
38
39
40
41
42
43
44
45
46
47
48
49
50
51
52
53
54
55
56
57
58
59
60

LH-ESI may facilitate high-throughput measurements of protein, protein complex, and protein-ligand thermochemistry, paving the way towards proteome-wide screening of the effect of ligands/drugs, buffers, growth conditions, or other treatments on protein thermal stabilities.

Supporting Information

Abundances of cyt *c* and BCAII as a function of solution temperature and laser power; Mass spectra and extracted ion chromatogram of BCAII before and after thermal cycling; Explanation of the two-protein calibration method for converting laser power to solution temperature; Modeling of the BF → U pathway using the theoretical abundance of U generated from two other U formation pathways.

Author Information

The authors declare no competing financial interests.

Author Contributions

JSJ and KJL performed all experiments. All coauthors contributed to the experimental design, data analysis, and the writing of the manuscript. ERW directed investigations.

References

1 R. Lumry and H. Eyring, *J. Phys. Chem.*, 1954, **58**, 110–120.
2 K. Huynh and C. L. Partch, *Curr. Protoc. Protein Sci.*, 2015, **79**, 28.9.1-28.9.14.
3 S. K. Chowdhury, V. Katta and B. T. Chait, *J. Am. Chem. Soc.*, 1990, **112**, 9013–9015.
4 Q. Wang, K.-C. Liang, A. Czader, M. N. Waxham and M. S. Cheung, *PLoS Comput. Biol.*, 2011, **7**, e1002114.
5 O. G. Hampe, *Eur. J. Biochem.*, 1972, **31**, 32–37.
6 R. L. Baldwin, *Biophys. J.*, 1996, **71**, 2056–2063.
7 F. Hofmeister, *Arch. Exp. Path. Pharma.*, 1888, **25**, 1–30.
8 F. Ahmad and C. C. Bigelow, *J. Protein Chem.*, 1986, **5**, 355–367.
9 S. Mittal and L. R. Singh, *J. Biochem.*, 2014, **156**, 273–282.
10 H. Dong, S. Qin and H. X. Zhou, *PLoS Comput. Biol.*, 2010, **6**, e1000833.
11 J. Roche, J. A. Caro, D. R. Norberto, P. Barthe, C. Roumestand, J. L. Schlessman, A. E. Garcia, B. García-Moreno E. and C. A. Royer, *PNAS*, 2012, **109**, 6945–6950.
12 G. Panick, R. Malessa, R. Winter, G. Rapp, K. J. Frye and C. A. Royer, *J. Mol. Biol.*, 1998, **275**, 389–402.
13 C. A. Royer, *Bioch. Biophys. Acta, Protein Struct. Mol. Enzym.*, 2002, **1595**, 201–209.
14 N. J. Greenfield, *Nat. Protoc.*, 2006, **1**, 2527–2535.
15 N. Poklar and G. Vesnaver, *J. Chem. Ed.*, 2000, **77**, 380.
16 C. A. Ross and M. A. Poirier, *Nat. Med.*, 2004, **10**, S10–S17.
17 N. Poklar, N. Petrovčič, M. Oblak and G. Vesnaver, *Protein Sci.*, 2008, **8**, 832–840.
18 G. C. Kresheck and J. E. Erman, *Biochemistry*, 1988, **27**, 2490–2496.
19 G. Wang, P. V. Bondarenko and I. A. Kaltashov, *Analyst*, 2018, **143**, 670–677.
20 J. Wen, H. Lord, N. Knutson and M. Wikström, *Anal. Biochem.*, 2020, **593**, 113581.
21 S. H. Kim, H. J. Yoo, E. J. Park and D. H. Na, *Pharmaceuticals*, 2021, **15**, 29.
22 T. O. C. Kwan, S. A. Kolek, A. E. Danson, R. I. Reis, I. S. Camacho, P. D. Shaw Stewart and I. Moraes, *Front. Mol. Biosci.*, 2022, **9**, 1–7.
23 J. A. J. Housmans, G. Wu, J. Schymkowitz and F. Rousseau, *FEBS J.*, 2023, **290**, 554–583.
24 J. J. Lavinder, S. B. Hari, B. J. Sullivan and T. J. Magliery, *J. Am. Chem. Soc.*, 2009, **131**, 3794–3795.
25 G. T. H. Nguyen, T. N. Tran, M. N. Podgorski, S. G. Bell, C. T. Supuran and W. A. Donald, *ACS Cent. Sci.*, 2019, **5**, 308–318.
26 G. T. H. Nguyen, W. Y. Leung, T. N. Tran, H. Wang, V. Murray and W. A. Donald, *Anal. Chem.*, 2020, **92**, 1130–1137.
27 G. T. H. Nguyen, A. Nocentini, A. Angeli, P. Gratteri, C. T. Supuran and W. A. Donald, *Anal. Chem.*, 2020, **92**, 4614–4622.
28 E. G. Báez Bolivar, D. T. Bui, E. N. Kitova, L. Han, R. B. Zheng, E. J. Luber, S. Y. Sayed, L. K. Mahal and J. S. Klassen, *Anal. Chem.*, 2021, **93**, 4231–4239.
29 E. N. Kitova, A. El-Hawiet, P. D. Schnier and J. S. Klassen, *J. Am. Soc. Mass Spectrom.*, 2012, **23**, 431–441.
30 G. T. H. Nguyen, J. L. Bennett, S. Liu, S. E. Hancock, D. L. Winter, D. J. Glover and W. A. Donald, *J. Am. Chem. Soc.*, 2021, **143**, 21379–21387.

31   D. D. Vallejo, C. Rojas Ramírez, K. F. Parson, Y. Han, V. V. Gadkari and B. T. Ruotolo, *Chem. Rev.*, 2022, **122**, 7690–7719.

32   A. Laganowsky, D. E. Clemmer and D. H. Russell, *Annu. Rev. Biophys.*, 2022, **51**, 63–77.

33   P. Leuenberger, S. Ganscha, A. Kahraman, V. Cappelletti, P. J. Boersema, C. von Mering, M. Claassen and P. Picotti, *Science*, 2017, **355**, eaai7825.

34   J. L. P. Benesch, F. Sobott and C. V. Robinson, *Anal. Chem.*, 2003, **75**, 2208–2214.

35   G. Wang, R. R. Abzalimov and I. A. Kaltashov, *Anal. Chem.*, 2011, **83**, 2870–2876.

36   T. J. El-Baba, D. W. Woodall, S. A. Raab, D. R. Fuller, A. Laganowsky, D. H. Russell and D. E. Clemmer, *J. Am. Chem. Soc.*, 2017, **139**, 6306–6309.

37   K. Jeanne Dit Fouque and F. Fernandez-Lima, *J. Phys. Chem. B*, 2020, **124**, 6257–6265.

38   D. W. Woodall, L. W. Henderson, S. A. Raab, K. Honma and D. E. Clemmer, *J. Am. Soc. Mass Spectrom.*, 2021, **32**, 64–72.

39   J. Liu, Y. Wang, X. Wang, W. Qin and G. Li, *Int. J. Mass Spectrom.*, 2023, **494**, 117151.

40   T. J. El-Baba and D. E. Clemmer, *Int. J. Mass Spectrom.*, 2019, **443**, 93–100.

41   R. B. J. Geels, S. Calmat, A. J. R. Heck, S. M. van der Vies and R. M. A. Heeren, *Rapid Commun. Mass Spectrom.*, 2008, **22**, 3633–3641.

42   C. J. Brown, D. W. Woodall, T. J. El-Baba and D. E. Clemmer, *J. Am. Soc. Mass Spectrom.*, 2019, **30**, 2438–2445.

43   M. M. Kostelic, J. P. Ryan, L. S. Brown, T. W. Jackson, C. Hsieh, C. K. Zak, H. M. Sanders, Y. Liu, V. S. Chen, M. Byrne, C. A. Aspinwall, E. S. Baker and M. T. Marty, *Anal. Chem.*, 2022, **94**, 11723–11727.

44   J. A. Harrison, A. Pruška, P. Bittner, A. Muck, D. A. Cooper-Shepherd and R. Zenobi, *Anal. Chem.*, 2022, **94**, 12435–12443.

45   L. W. Henderson, E. M. Sharon, A. K. S. Gautam, A. J. Anthony, M. F. Jarrold, D. H. Russell, A. Matouschek and D. E. Clemmer, *J. Phys. Chem. Lett.*, 2023, **14**, 5014–5017.

46   C. W. Lin, S. D. Oney-Hawthorne, S. T. Kuo, D. P. Barondeau and D. H. Russell, *Biochemistry*, 2022, **61**, 2733-2741.

47   A. Marchand, M. F. Czar, E. N. Eggel, J. Kaeslin and R. Zenobi, *Nat. Commun.*, 2020, **11**, 566.

48   A. Pruška, J. A. Harrison, A. Granzhan, A. Marchand and R. Zenobi, *Anal. Chem.*, 2023, **95**, 14384–14391.

49   A. Marchand, F. Rosu, R. Zenobi and V. Gabelica, *J. Am. Chem. Soc.*, 2018, **140**, 12553–12565.

50   X. Cong, Y. Liu, W. Liu, X. Liang, D. H. Russell and A. Laganowsky, *J. Am. Chem. Soc.*, 2016, **138**, 4346–4349.

51   T. Walker, H. M. Sun, T. Gunnels, V. Wysocki, A. Laganowsky, H. Rye and D. Russell, *ACS Cent. Sci.*, 2023, **9**, 466–475.

52   S. A. Raab, T. J. El-Baba, D. W. Woodall, W. Liu, Y. Liu, Z. Baird, D. A. Hales, A. Laganowsky, D. H. Russell and D. E. Clemmer, *J. Am. Chem. Soc.*, 2020, **142**, 17372–17383.

53   H. Pan, S. A. Raab, T. J. El-Baba, S. R. Schrecke, A. Laganowsky, D. H. Russell and D. E. Clemmer, *J. Phys. Chem. A*, 2023, **127**, 9399–9408.

54   T. J. El-Baba, S. A. Raab, R. P. Buckley, C. J. Brown, C. A. Lutomski, L. W. Henderson, D. W. Woodall, J. Shen, J. C. Trinidad, H. Niu, M. F. Jarrold, D. H. Russell, A. Laganowsky and D. E. Clemmer, *Anal. Chem.*, 2021, **93**, 8484–8492.

55   F. Zhao, S. M. Matt, J. Bu, O. G. Rehrauer, D. Ben-Amotz and S. A. McLuckey, *J. Am. Soc. Mass Spectrom.*, 2017, **28**, 2001–2010.

56   X. Shi, A. Takamizawa, Y. Nishimura, K. Hiraoka and S. Akashi, *Rapid Commun. Mass Spectrom.*, 2008, **22**, 1430–1436.

57   X. Shi, A. Takamizawa, Y. Nishimura, K. Hiraoka and S. Akashi, *J. Mass Spectrom.*, 2006, **41**, 1086–1095.

58   J. S. Jordan and E. R. Williams, *Anal. Chem.*, 2022, **94**, 16894–16900.

59   T. J. El-Baba, D. R. Fuller, D. W. Woodall, S. A. Raab, C. R. Conant, J. M. Dilger, Y. Toker, E. R. Williams, D. H. Russell and D. E. Clemmer, *Chem. Commun.*, 2018, **54**, 3270–3273.

60   A. Takamizawa, Y. Itoh, R. Osawa, N. Iwasaki, Y. Nishimura, S. Akashi and K. Hiraoka, *J. Mass Spectrom.*, 2004, **39**, 1053–1058.

61   H. J. Sterling and E. R. Williams, *J. Am. Soc. Mass Spectrom.*, 2009, **20**, 1933–1943.

62   J. S. Jordan, Z. Xia and E. R. Williams, *J. Am. Soc. Mass Spectrom.*, 2022, **33**, 607–611.

63   D. N. Mortensen and E. R. Williams, *Anal. Chem.*, 2014, **86**, 9315–9321.

64   J. S. Jordan, Z. M. Miller, C. C. Harper, E. Hanozin and E. R. Williams, *J. Am. Soc. Mass Spectrom.*, 2023, **34**, 1186–1195.

65   M. L. Williams, *Occup. Environ. Med.*, 1996, **53**, 504–504.

66   V. M. Krishnamurthy, G. K. Kaufman, A. R. Urbach, I. Gitlin, K. L. Gudiksen, D. B. Weibel and G. M. Whitesides, *Chem. Rev.*, 2008, **108**, 946–1051.

67   A. Sharma, R. Chiang, M. Manginell, I. Nardi, E. N. Coker, J. M. Vanegas, S. B. Rempe and G. D. Bachand, *ACS Omega*, 2023, **8**, 37830–37841.

68   L. F. Schachner, A. N. Ives, J. P. McGee, R. D. Melani, J. O. Kafader, P. D. Compton, S. M. Patrie and N. L. Kelleher, *J. Am. Soc. Mass Spectrom.*, 2019, **30**, 1190–1198.

69   H. Zhang, W. Cui and M. L. Gross, *Int. J. Mass Spectrom.*, 2013, **354–355**, 288–291.

70   F. Yang, B. R. Zhou, P. Zhang, Y. F. Zhao, J. Chen and Y. Liang, *Chem. Biol. Interact.*, 2007, **170**, 231–243.

71   N. S. Sarraf, A. A. Saboury, B. Ranjbar and A. A. Moosavi-Movahedi, *Acta Biochim. Pol.*, 2004, **51**, 665–671.

72   F. Azari and M. Nemat-Gorgani, *Biotechnol. Bioeng.*, 1999, **62**, 193–199.

73   S. Bhattacharya, M. Schiavone, S. Chakrabarti and S. K. Bhattacharya, *Biotechnol. Appl. Biochem.*, 2003, **38**, 111.

74   C. Capasso, V. De Luca, V. Carginale, P. Caramuscio, C. F. N. Cavalheiro, R. Cannio and M. Rossi, *Chem. Eng. Trans.*, 2012, **27**, 271–276.

75   L. Alaei, A. A.Moosavi-Movahedi, H. Hadi, A. A. Saboury, F. Ahmad and M. Amani, *Protein Pept. Lett.*, 2012, **19**, 852–858.

76   K. L. Davidson, D. R. Oberreit, C. J. Hogan and M. F. Bush, *Int. J. Mass Spectrom.*, 2017, **420**, 35–42.

77   A. C. Susa, Z. Xia and E. R. Williams, *Anal. Chem.*, 2017, **89**, 3116–3122.

78   J. S. Jordan and E. R. Williams, *Anal. Chem.*, 2021, **93**, 1725–1731.

79   J. S. Jordan and E. R. Williams, *Analyst*, 2021, **146**, 6822–6830.

80   M. F. Drenski, M. L. Brader, R. W. Alston and W. F. Reed, *Anal. Biochem.*, 2013, **437**, 185–197.

81   V. A. Borzova, K. A. Markossian, N. A. Chebotareva, S. Y. Kleymenov, N. B. Poliansky, K. O. Muranov, V. A. Stein-Margolina, V. V. Shubin, D. I. Markov and B. I. Kurganov, *PLoS One*, 2016, **11**, e0153495.
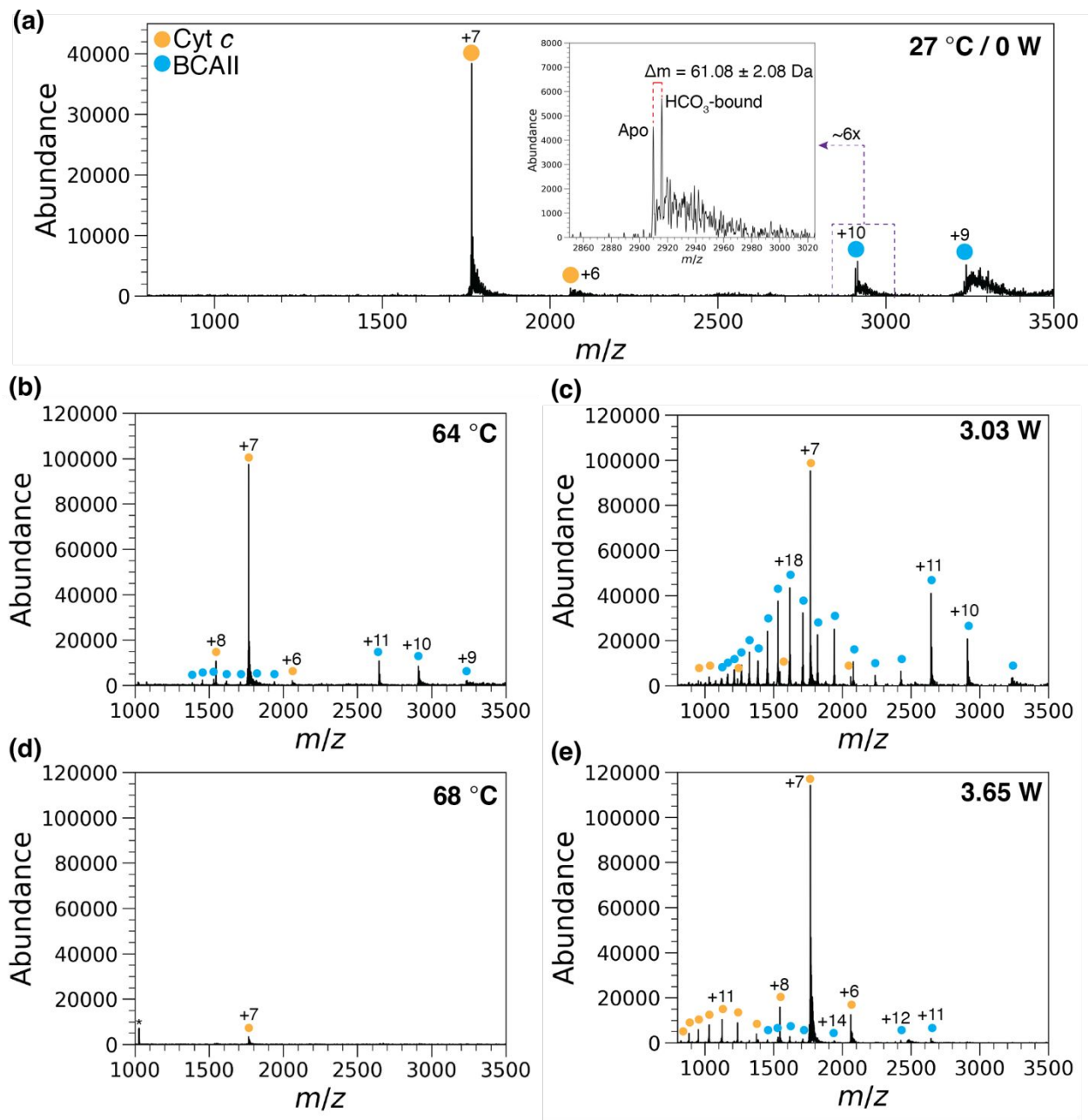
Figure 1. (a) Native ESI mass spectra of a 7:3 BCAII:Cyt *c* mixture (10 µM total protein

concentration) in 50 mM ammonium acetate at room temperature. The inset shows the region

between $m/z = 2850 – 3025$, highlighting apo-BCAII and bicarbonate-bound species. (b,d) vT-ESI mass spectra of the BCAII:Cyt c mixture acquired at solution temperatures of 64 °C and 68 °C. (c,e) LH-ESI mass spectra of the same sample acquired at laser powers of 3.03 W and 3.65 W by heating only the final 300 μm of the emitter.
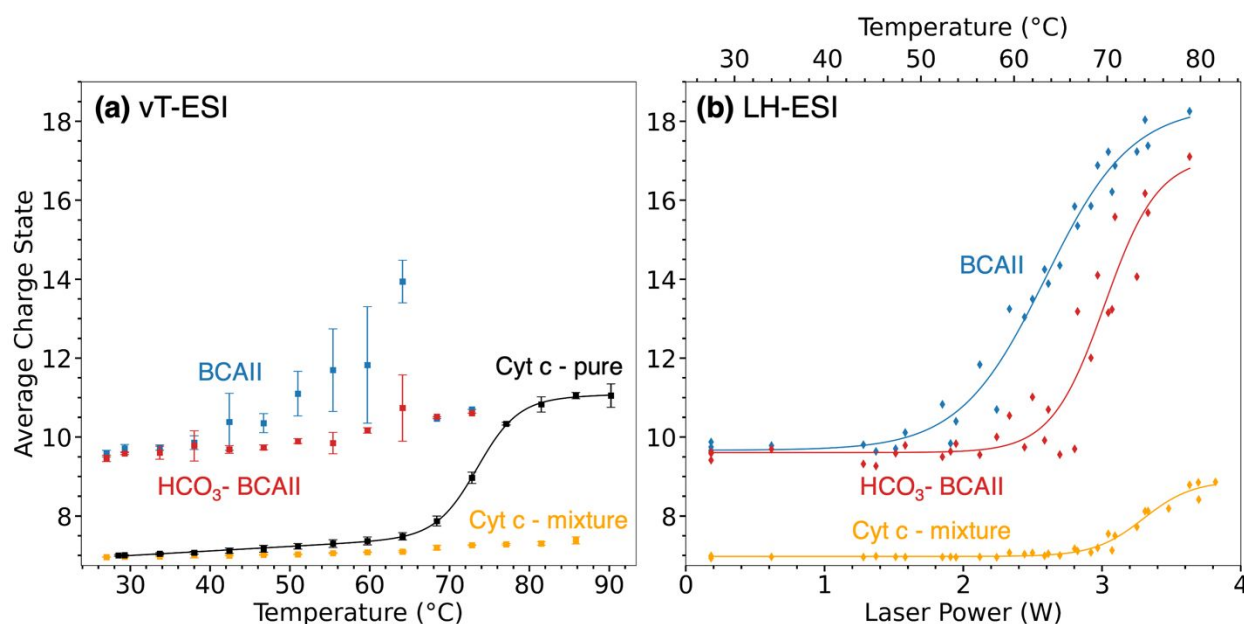
Figure 2. Average charge state of apo- and bicarbonate-bound BCAII (blue/red) and cyt c (orange/black) obtained by (a) vT-ESI or (b) LH-ESI from a solution containing 7:3 BCAII:cyt c in 50 mM ammonium acetate. LH-ESI data are shown as a function of laser power (bottom axis) and recalibrated temperature (top axis). BCAII signal above ~68 °C in (a) was observed in only one replicate. Data in black were obtained from a solution containing 10 μM cyt c in 20 mM ammonium acetate. There are no BCAII ions above ~72 °C in vT-ESI experiments due to irreversible aggregation, preventing the measurement of a full melting curve for this protein.
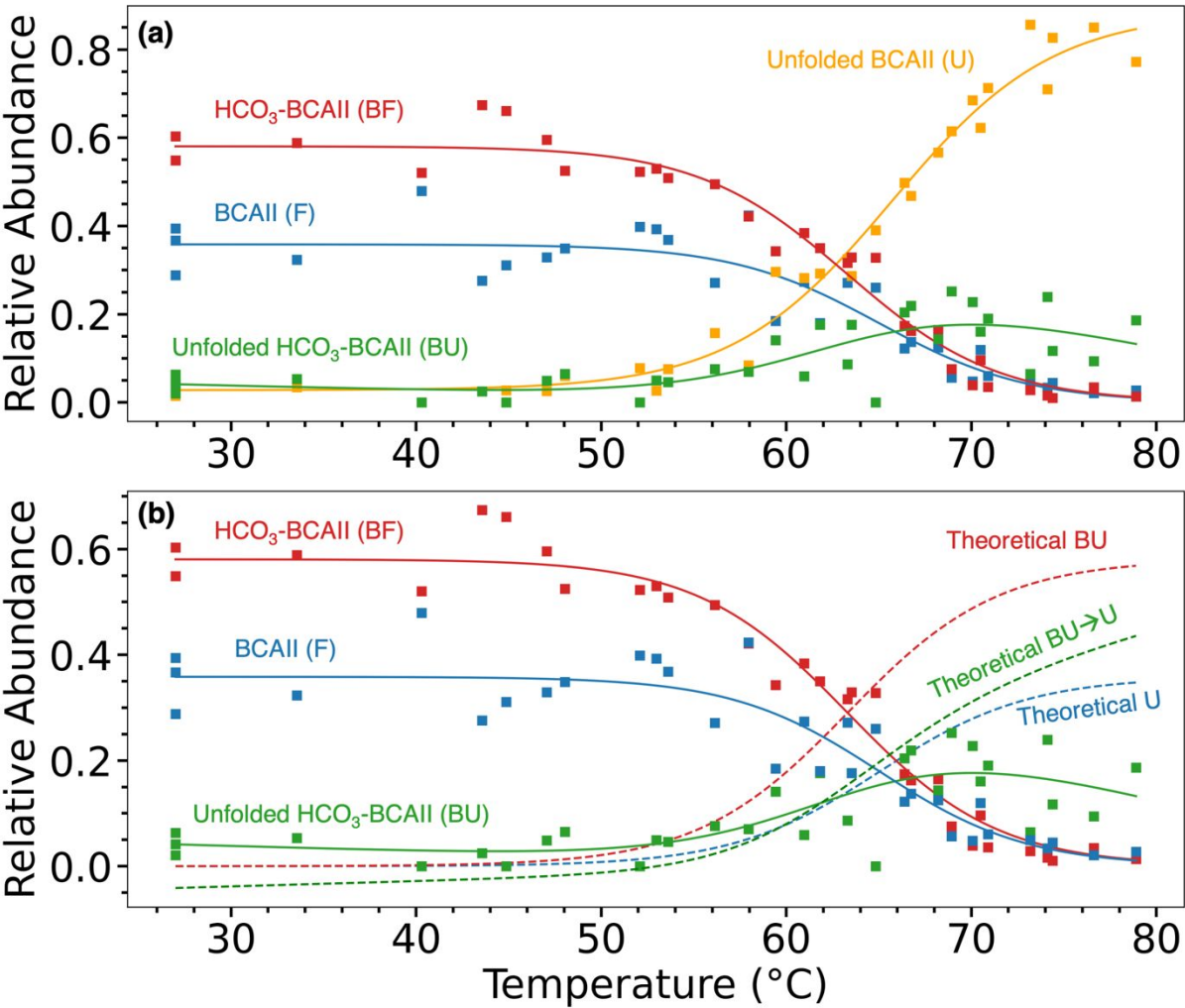
Figure 3. (a) LH-ESI melting curves of the native (charge states +8 - +10) and denatured (charge states +11 - +31) forms of bicarbonate-bound and apo-BCAII measured by the population abundances of the different forms and (b) including the modeled abundances (dashed lines) of BU, U, and U that is formed by loss of bicarbonate from BU (BU→U).
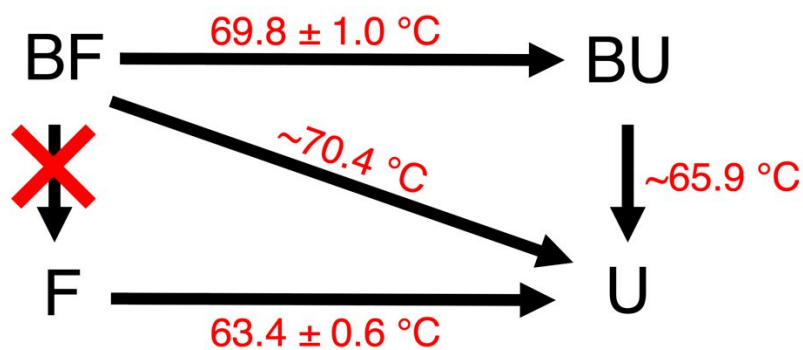
Scheme 1. Possible mechanisms of bicarbonate loss from BCAII and the associated T_m value for each of the processes (shown in red above each arrow). Conversion of the folded bicarbonate-bound protein to folded apo-protein is not observed. BF = bicarbonate-bound folded protein; BU = bicarbonate-bound unfolded protein; F = folded apo-protein; U = unfolded apo-protein.